Lasers in Manufacturing Conference 2025

Determining the individual structural strength of three-dimensional macrostructures as a function of ambient pressure

Christian Frey[a*], Abhay Sharma[a], Pia Fischer[b†], Benjamin Gerhards[c], Simon Olschok[a], Christian Hopmann[b], Uwe Reisgen[a]

[a]*Welding and Joining Institute (ISF), RWTH Aachen University, Pontstrasse 49, 52062 Aachen, Germany*
[b]*Insitute for Plastics Processing (IKV) at RWTH Aachen University, Seffenter Weg 201, 52074 Aachen, Germany*
[c]*LaVa-X GmbH, Kaiserstrasse 100, 52134 Herzogenrath, Germany*
[*]*Corresponding Author: christian.frey@isf.rwth-aachen.de*
[†]*Previously published as Pia Wagner*

Abstract

Conventionally, metals and plastics compete due to their differing mechanical, physical, chemical, and tribological properties. However, hybrid components that synergistically utilize the advantages of both materials present significant potential for weight reduction, functional integration, and cost savings. The production of plastic/metal hybrid components can be efficiently achieved during the primary forming process of the plastic part by back-molding thus eliminating the need for additional joining technologies using form closure through macrostructures. Macro structuring on metal components is accomplished through laser or electron radiation via repeated micro-welds (Surfi-Sculpt®). The strength of these structures can be tailored by adjusting process parameters, orientation, and geometry of the micro-welds. This study presents initial results regarding individual structural strength on stainless steel samples. It demonstrates the dependency of bending strength and structure geometry on ambient pressure as well as the increase in structural strength in welding direction. Higher energy input allows for elevated macrostructures but may reduce bending strength.

Keywords: Back-molding ; form-closure joining ; injection molding ; laser welding ; LaVa ; plastic-metal-hybrids ; Surfi-Sculpt®

1. Introduction

According to Dröder, 2019, hybrid plastic-metal components are increasingly adopted in industries such as automotive and aerospace due to their potential for weight reduction, cost efficiency and tailored mechanical performance. While the mechanical properties of metals and the design flexibility of plastics offer complementary advantages, their inherent differences in thermal expansion, stiffness and bonding mechanisms present significant joining challenges, as discussed by Amancio-Filho et al., 2009. Plastic/metal hybrid components can be manufactured post-mold, for example by welding, or in-mold during the initial forming process of the plastic component. Compared to welding processes, in-mold assembly does not require any additional joining technology and the usable bonded area can be designed more flexibly, as seen in Finnah, 2005. According to Drossel et al., 2016, the structured metal component is inserted into the injection mold, back-molded with the plastic component, and joined simultaneously, eliminating the need for an additional joining step. The produced hybrid components are ready for use without any further processing. The most commonly used connecting mechanisms in established hybrid technology are form closure and adhesion. Due to the low creep resistance of plastics, Amancio- Filho et al., 2009 states that a pure force connection between the two materials is not possible long term. Banea et al., 2018 explains that adhesive bonding, though simple and cost-effective, is sensitive to surface conditions, thermal aging, and generally offers limited material combinations. In the simplest case, as seen in the work of Geminger et al., 2016, holes are

manufactured into the metal component through which the molten plastic can flow, creating a rivet-like fastener or a form-fitting connection by injection molding around the edges of the metal component. However, Amancio-Filho et al. 2009 argues that using these connection techniques results in uneven, localized stress peaks, which need to be balanced by over-dimensioning component parts.

Alternative methods include laser micro structuring by laser ablation mentioned in Heckert et al., 2014 and Rösner, 2014, laser remelting as seen in Temmler et al., 2017, vacuum suction blasting present in Ruhland, 2004 and Staiger et al., 2014, or special etching processes referred to in Vasconcelos et al., 2023, which form structures in the metal surface with sometimes undercuts that can be used for a form-fitting connection by back-molding. In contrast to those processes, which structure wide areas, Blackburn and Hilton, 2011 explain that the Surfi-Sculpt® process generates individual micro-weld seams on the surface through remelting material. Due to a relative movement of the beam in relation to the workpiece, Dance et al., 2007 explains that the melt flows around a capillary and solidifies on the side facing away from the movement. By repeating this step several times at the same position, the material is layered on top of itself, creating a raised surface structure (elevation) with a larger aspect ratio (height to depth) and a cavity on the other side, as presented in Figure 1 and shown by Earl et al., 2012. Experiments by Wang et al., 2015 and Gach et al., 2019 show that depending on the beam movement, freely programmable structures can be created to form a three-dimensional surface.

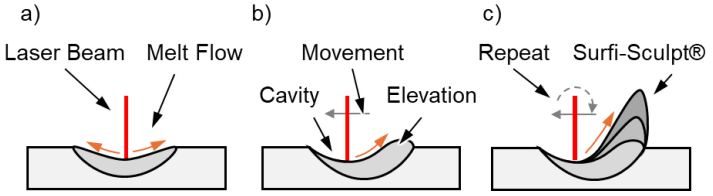

Figure 1: Schematic view of the process by a laser beam showing a) the initial start, b) the first movement and c) the Surfi-Sculpt® structure through repeated movement

Wurzbacher et al., 2021 demonstrate that the resulting three-dimensional surface offers the potential to utilize as form closure in plastic/metal hybrid components by back-molding in a load-specific manner and achieve improved and precisely controllable force transmission. However, Blackburn and Hilton, 2011 emphasize that precise heat management during the Surfi-Sculpt® structuring process is crucial to create large structures that do not suffer from overheating. Earl et al., 2012 suggest that at higher ambient pressures, convective heat dissipation is more effective, leading to faster cooling, a more viscous melt and ultimately larger and more stable structures. On the other side, Frey et al., 2024 mention that a higher ambient pressure also increases the evaporation temperature of the material leading to higher process temperatures and wider weld seams. The relation between reduced pressure and temperature has been explored by Honig et al., 1969, where for example, reducing the ambient pressure to 10 mbar leads to a temperature drop by 766 K , which reduces the average temperature of the capillary wall, as explained by Li et al. 2018. Therefore, this study investigates the previously unexplored area between the structuring with an electron beam in high vacuum (10^{-4} mbar) and the laser structuring in atmosphere through laser structuring in between 1–1,000 mbar, with a focus on determining and optimizing individual structure strength.

2. Experimental Procedure

The LaVaCELL450 used for producing Surfi-Sculpt® structures contains a 2 kW singlemode SPI redPower CUBE laser with a diffraction index M^2 of 1.1. The connected Raylase SuperScan IV-30 Optic achieves a spot diameter of 52.88 µm and a Rayleigh length of 1.87 mm due to the 423 mm F-Theta objective alongside a Collimator of 200 mm. This optical system connects to a 90 liter vacuum chamber. The surface structuring was carried out with a laser power of 480 W, a focus position 5 mm below the workpiece surface and a welding speed of 1,200 mm/s at three different pressure levels of 10 mbar, 100 mbar and 1,000 mbar. For each pressure level, the argon shielding gas flow was adapted to 5 l/min, 10 l/min and 20 l/min, respectively.

The structuring was performed on a 27 mm wide, 100 mm long and 2 mm thick 304 stainless steel plate (1.4301) with 50 and 100 repetitions. To prevent thermal overheating of the individual structures, the length of the weld seam was set to 4 mm and the repetition for all structures were simultaneously produced. For every parameter combination, ten structures were formed and tested for their individual load bearing capacities in three directions – 0°, 90° and 180°, where 0° represents the welding direction, as seen in Figure 2 a).

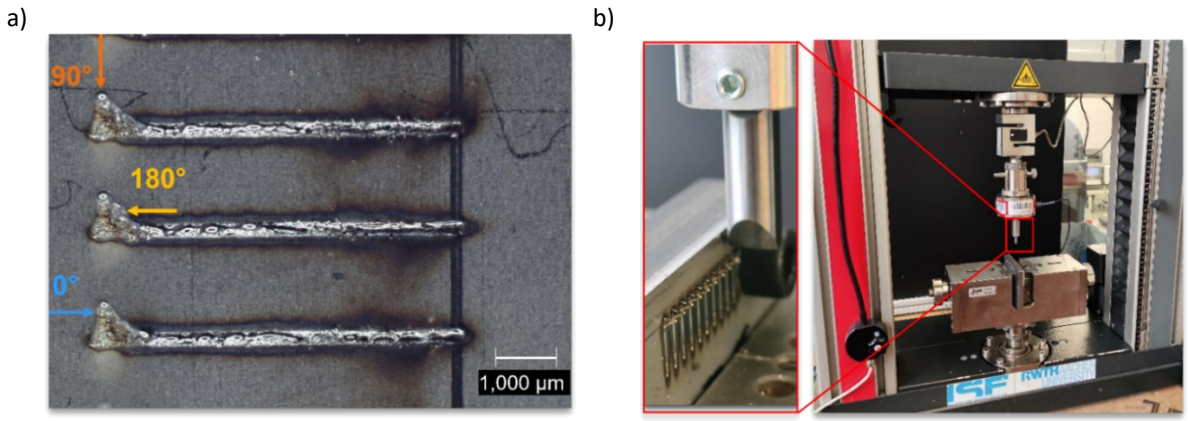

Figure 2: a) Definition of testing direction shown on structures produced at 100 mbar with 50 repetitions and b) used Zwick/Roell Z010 RetroLine universal testing machine with applied test pin 0.4 mm above the workpiece surface shown for 0° testing direction

The bending test was carried out using a Zwick/Roell Z010 RetroLine universal testing machine with a 100 N load cell and a testing speed of 10 mm/min. The force was applied at a constant distance of 0.4 mm above the workpiece surface for all generated structures, as demonstrated in Figure 2 b).

3. Results and discussion

Besides Figure 2 a), which illustrates the structures for n = 50 repetitions and p = 100 mbar, Figure 3 b) and c) show the formed structures for 50 and 100 repetitions at a working pressure of 10 mbar. In comparison, the geometric shape of the structure mainly changes in the direction of height depending on the working pressure. In addition, there are more deposits next to the structure at 10 mbar compared to 100 mbar in form of discoloration. The structures at 1,000 mbar are significantly less consistent and represent an unstable process, resulting in heavy spatter deposits and partial collapse of the structures for 100 repetitions as shown in Figure 3 a). Therefore, only the repetition rate of n = 50 at 1,000 mbar is considered for further analyzation.

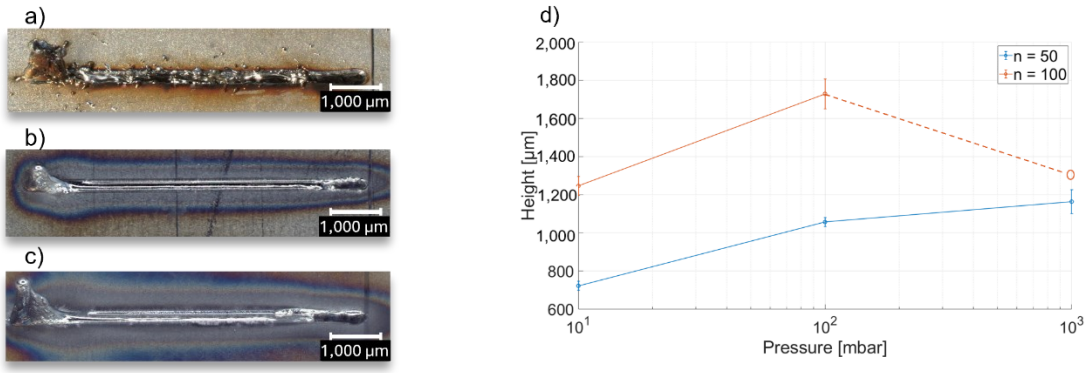

Figure 3: a) Laser microscope images of Structures produced at a) 1,000 mbar with 100 repetitions, b) 10 mbar with 50 repetitions and c) 10 mbar with 100 repetitions as well as d) measured height over pressure for 50 and 100 repetitions

The measured structure height for different repetition rates over the working pressure are summarized in Figure 3 d). Each data point represents the mean value of ten structures except the data point for n = 100 and p = 1,000 mbar. This value shows an exemplary single measurement of a collapsed structure, thereby not representing the achievable height. Adapted heat management could be a solution here. However, an increasing number of repetitions leads to greater average structure height, which is consistent with the expectation that repeated passes of the laser result in increased material displacement and accumulation. In addition, a positive correlation between the ambient pressure and structure height is evident for both repetition rates. This supports the hypothesis that a higher working pressure enhances convective heat dissipation, allowing more rapid cooling of the melt pool and thus enabling the formation of taller structures.

The maximum measured force of the formed structures, depending on the testing direction of 0°, 90° and 180°, is shown in Figure 4. The highest force can be absorbed predominantly in 0° (welding direction), with a maximum at 100 mbar. Structures with 100 repetitions exhibit marginally improved maximum force compared to 50 repetitions. This can be

attributed to their increased height and structural mass. While the maximum force at 100 mbar suggests the presence of an optimal pressure due to a balance between effective heat dissipation and reduced evaporation temperature. The evaporation temperature of iron, present in Honig et al., 1969 is approximately 3,081 K at 1,000 mbar, while dropping to 2,628 K and 2,315 K for 100 mbar and 10 mbar, respectively. At 10 mbar, insufficient cooling likely compromises the structural integrity, while at 1,000 mbar, the higher process temperature and the presence of residual oxygen may reduce the structural strength. Since the structures collapsed at 1,000 mbar and 100 repetitions, the measured maximum force is only an indicative and therefore differently marked. The actual force could be lower since the collapsed structures are wider which results into more resisting material.

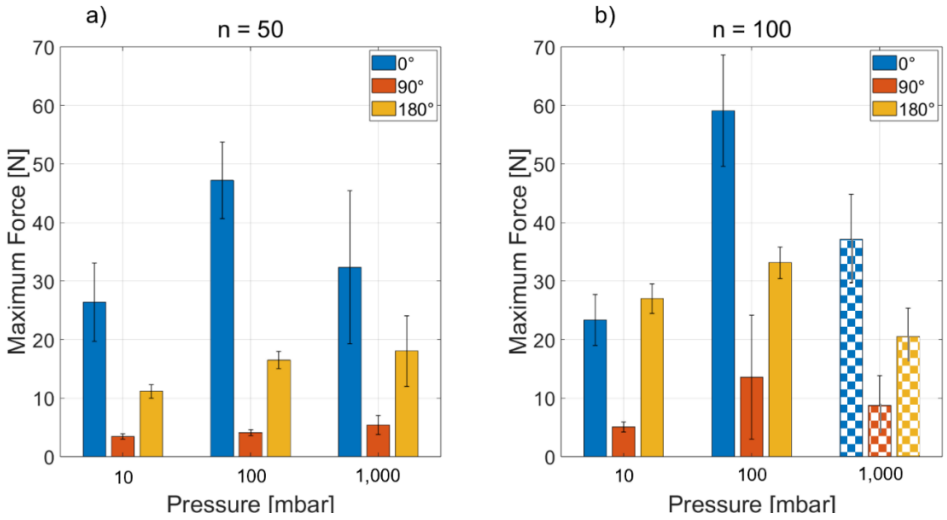

Figure 4: Maximum measured force of each testing direction over pressure for a) 50 repetitions and b) 100 repetitions

The individual structural strength is determined by normalizing the measured force of each testing direction (0°, 90°, 180°) to the maximum force in this series. Figure 5 a) shows the force that the structures can absorb depending on the direction. The structures resist the highest force in 0° testing direction, with decreased performance for 90° and intermediate results for 180°. An exception indicates the structures at 10 mbar, which absorb the maximum force at 180°, but also resist almost identical performance at 0°. At 90°, all structures present less than 25 % of the maximum force.

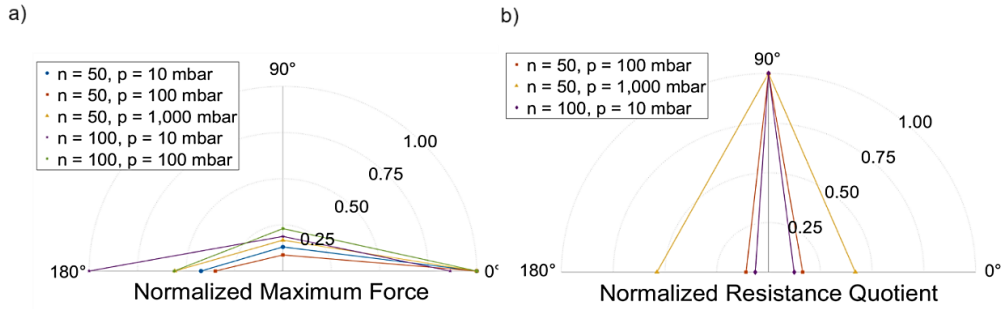

Figure 5: Individual structure strength shown for a) normalized to maximum force and b) normalized to the second moment of area (2nd MOA)

However, Figure 5 a) neglects that the second moment of area (2nd MOA), which indicates the resistances of each structure, varies depending on the test direction. The simplified cross section of the structures refers to a rectangular each of which has a 2nd MOA in the x- and y-direction. At 90°, the structure width is included in the calculation to the power of three, while at 0° and 180°, the structure length is decisive as illustrated in Figure 6. This implies that the 2nd MOA for 90° test direction is significantly smaller compared to 0° and 180°.

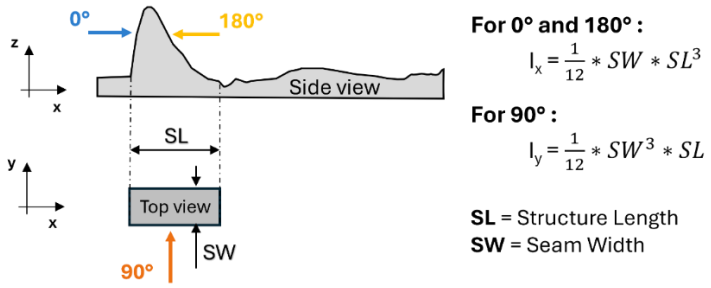

Figure 6: Calculated 2nd MOA in the x- and y-direction of the structures with the assumption of a rectangular cross section

By dividing the measured force through the 2nd MOA of the corresponding structure, a resistance coefficient is formed. This coefficient is normalized to the maximum value as shown in Figure 5 b). In this representation, the greatest resistance of the structures is in 90° testing direction. Consequently, a strong parallelization of several structures within a hybrid connection as presented in Wurzbacher et al., 2021 could exhibit greater joint strength at 90°. Thus, the hybrid connection with 20 parallel structures has only been measured at 0° and 180°.

Besides the individual maximum force, the different force-strain curves, as shown in Figure 7 a), indicate various failure behaviors, which is why Figure 7 b) presents the tested structures for 100 mbar and 50 repetitions depending on the test direction. For the 0° testing direction, the tested structures primarily exhibit shear displacement followed by bending. The 180° test direction resulted also in shear followed by bending, while the 90° test direction primarily presents a bending deformation of the structure. The same can be confirmed by the force/strain curves, where the 0° test showed a steep increase in the applied force signifying the shearing phenomena followed by a plateauing of the force corresponding to bending. Similarly, the 90° test showed significant plateauing of the force, which is associated with the almost pure bending behavior of the elevation. As the distance from the point of force application remained constant (0.4 mm above the surface) across all tests, it can be inferred that the failure mechanism is highly dependent on the relative direction of the applied force with respect to the elevation orientation. Grain orientation induced by the welding direction may further influence this behavior.

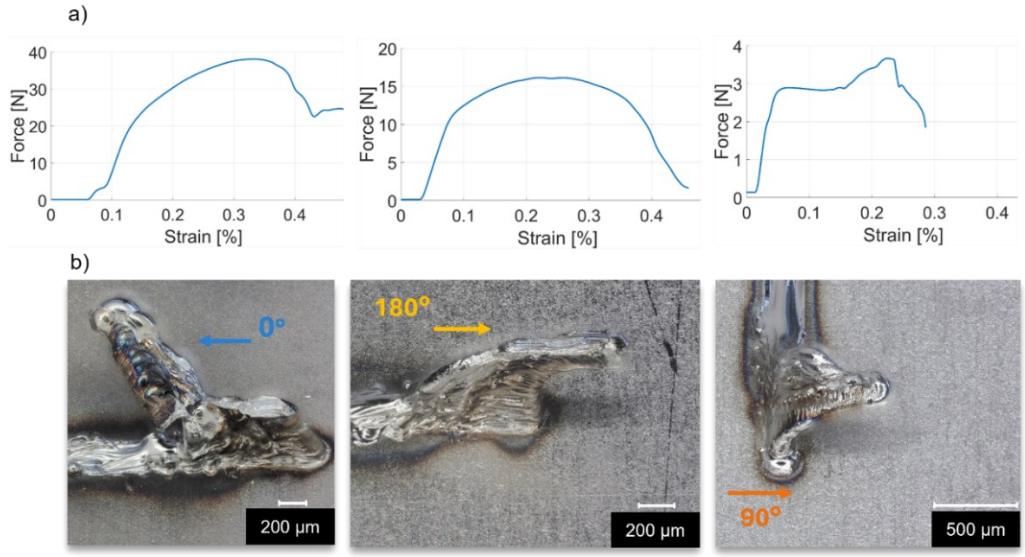

Figure 7: a) Samples of a measured force-strain for 100 mbar and 50 repetitions at testing direction 0°, 180°, and 90 as well as b) corresponding laser microscopy images of the structures after testing

4. Conclusion

This study investigated the influence of ambient pressure and laser processing parameters on the structural integrity and mechanical performance of individual Surfi-Sculpt® structures formed on stainless steel 304 (1.4301). Based on the experimental results, the following conclusions can be drawn:

- The structure height increases with the number of laser repetitions, as more passes lead to additional material displacement and accumulation.
- Higher ambient pressure promotes the formation of taller structures by enhancing the convective cooling, which facilitates more effective solidification of the melt pool.
- A working pressure of 100 mbar provides the best balance between structure formation and mechanical strength, suggesting an optimal range for thermal management and structure quality.
- The mechanical failure mode of the structure is highly dependent on the test direction of the applied force which leads to a mixture of shearing and bending of the structures.
- The maximum force of the structures is measured in 0° test direction, followed by 180° followed by 90°.
- The greatest resistance in relation to 2nd MOA results in 90°.

These insights offer valuable guidance for tailoring the design and processing of form-fit structures in hybrid plastic-metal components, especially for applications requiring additional directional strength and optimized performance under varying ambient conditions. Therefore, the next steps investigate how the individual structure strength relates to the overall strength of the plastic/metal hybrid components.

Acknowledgements

The presented work was funded by the Deutsche Forschungsgemeinschaft (DFG, German Research Foundation) – Project number 555232518. We would like to extend our thanks to the DFG.

References

Dröder, K., 2019. Technologies for economical and functional lightweight design. Springer Vieweg, Germany.

Amancio Filhio, S.T., dos Santos, J.F., 2009. Joining of Polymers and Polymer-Metal Hybrid Structures: Recent Developments and Trends. Polymer Engineering & Sci 49. DOI: 10.1002/pen.21424.

Finnah, G. 2005. Verfahrensentwicklungen beim Mehrkomponenten-Spritzgießen zur Herstellung von keramischen und metallischen Mikrobauteilen [Dissertation]. Albert-Ludwigs-Universität, Freiburg im Breisgau, Germany.

Drossel, W.G., Lies, C., Albert, A., Haase, R., Müller, R., Scholz, P., 2016. Process combinations for the manufacturing of metal-plastic hybrid parts. IOP Conference: Mater. Sci. Eng. DOI: 10.1088/1757-899X/118/1/012042.

Banea, M.D., Da Silva, L.F.M., Campilgo, R.D.S.G., 2018. Principles of Adhesive Bonding. Part I - Joining Processes Based on Adhesion Forces, in "Joining of Polymer–Metal Hybrid Structures: Principles and Applications" Amancio-Filho, S.T., Blaga, L.A., Editor. John Wiley & Sons, Inc.

Geminger, T., Jarka, S., 2016. Injection Molding of Multimaterial Systems, in "Specialized Injection Molding Techniques" Heim, H.P., Editor. Elsevier, Amsterdam, p. 165-210

Heckert, A., Zaeh, M.F., 2014. Laser Surface Pre-treatment of Aluminium for Hybrid Joints with Glass Fibre Reinforced Thermoplastics. Physica Procedia 56. DOI: 10.1016/j.phpro.2014.08.032.

Rösner, A., 2014. Laserbasiertes Fügeverfahren zur Herstellung von Kunststoff-Metall-Hybridbauteilen [Dissertation]. Fraunhofer-Institut für Lasertechnik ILT, Stuttgart. Fraunhofer Verl. 2014

Temmler, A., Küpper, M., Walochnik, M.A., Lanfermann, A., Schmickler, T., Bach, A., et al, 2017. Surface Structuring by laser remelting of metals. Journal of Laser Applications 29. DOI: 10.2351/1.4972414.

Ruhland, S. 2004. Vakuum-Saugstrahlen in der Fertigungslinie. J. Oberfl. Techn. 44, p. 50-52. DOI: 10.1007/BF03240878.

Staiger, E., Hild, M., Hund, R.D., Cherif, C., Bräunling, S., Hardtmann, A., 2014. Oberflächen haftungsgerecht gestalten. Adhäsion KLEBEN & DICHTEN 58, p. 32-35. DOI: 10.1365/s35145-014-0488-8

Vasconcelos, R.L., Oliveira, G.H.M., Amancio-Filho, S.T., Canto, L.B., 2023. Injection overmolding of polymer-metal hybrid structures: A review. Polymer Engineering & Sci 63, p. 691-722. DOI: 10.1002/pen.26244.

Blackburn, J., Hilton, P., 2011. Producing Surface Features with a 200 W Yb-fibre Laser and the Surfi-Sculpt® Process. Physics Procedia 12, p. 529-536. DOI: 10.1016/j.phpro.2011.03.065.

Dance, B.G.I., Buxton, A.L., 2007. An Introduction to Surfi-Sculpt Technology - New Opportunities, New Challenges. 7th International Conference on Beam Technology, Halle, Germany.

Earl, C., Hilton, P., O'Neill, B., 2012. Parameter Influence on Surfi-Sculpt Processing Efficiency. Physics Procedia 39, p. 327–35. DOI: 10.1016/j.phpro.2012.10.045.

Wang, X., Ahn, J., Bai, Q., Lu, W., Lin, J., 2015. Effect of forming parameters on electron beam Surfi-Sculpt protrusion for Ti–6Al–4V. Materials & Design 76, p. 202-206. DOI: 10.1016/j.matdes.2015.03.065.

Gach, S., Olschok, S., Reisgen, U., 2019. Geometric modulation of microscale surface structures for defined stimulation of osteogenic differentiation on implant materials. Materialwiss. Werkstofftech. 50, p. 365–371. DOI: 10.1002/mawe.201800168.

Wurzbacher, S., Gach, S., Reisgen, U., Hopmann, C., 2021. Joining of plastic-metal hybrid components by overmoulding of specially designed form-closure elements. Materialwiss. Werkstofftech. 52, p. 367–378. DOI: 10.1002/mawe.202000158.

Frey, C., Beyel, A., Wahl, J., Twiehaus, T., Olschok, S., Hagenlocher, C., et al., 2024. Interdependence of metal vapor plume and melt pool dynamics during laser beam welding under vacuum. Journal of Laser Applications 36. DOI: 10.2351/7.0001557.

Honig, R.E., Krammer, D.A., 1969. Vapor data pressure for the solid and the liquid elements. RCA Review 30, p. 285–305.

Li, L., Peng, G., Wang, J., Gong, J., Meng, S., 2018. Numerical and experimental study on keyhole and melt flow dynamics during laser welding of aluminium alloys under subatmospheric pressures. International Journal of Heat and Mass Transfer 133, p. 812–826. DOI: 10.1016/j.ijheatmasstransfer.2018.12.165.